Ripple formation on a particle bed sheared by a viscous liquid. Part 2. Oscillating flow

By F. CHARRU[1] and E. J. HINCH[2]

[1]IMFT, Allée C. Soula, 31400 Toulouse, France

[2]Department of Applied Mathematics and Theoretical Physics, University of Cambridge, Wilberforce Road, Cambridge CB3 0WA, UK

A new model for the erosion and deposition of particles, developed in Part 1, is now applied to oscillating flows to give an analytic expression for the growth rate. We find that ripples can grow in oscillating flows when they do not in steady flows of the same magnitude, this being due to a suppression in rapidly oscillating flows of the erosion by higher shear rates on the crests.

1. Introduction

It is well-known that an oscillating flow over a sandy bottom, such as that induced by a surface wave in shallow water, creates sand ripples (Bagnold 1946). The commonly accepted explanation is that these ripples result from an instability of the fluid flow: over an initial spatially periodic bed disturbance, there exists an inertially induced mean fluid flow, or steady streaming, which is directed from troughs to crests (Sleath 1976; Kaneko & Honji 1979). This steady streaming drags the particles towards crests, thus amplifying the initial bed disturbance. All wavenumbers are unstable, but the component of gravity parallel to the wavy bed stabilizes the smallest and highest ones, resulting in a finite-wavenumber instability (Blondeaux 1990). However, there is no clear experimental evidence that this mechanism is the dominant one: a crucial test for stability theories is the measurement of growth rates, but such measurements are lacking. Moreover, the facts that the shape seems far from sinusoidal (Stegner & Wesfreid 1999) and that coalescence occurs at the early stages of growth (Faraci & Foti 2001) indicate that linear stability theories might be of little use. A quite different approach has been developed by Andersen (2001), who considers the ripples as small packets of particles distributed over the bed, interacting through the wakes. This approach is able to reproduce ripple coalescence, with the predicted wavelength in reasonable agreement with experiments. Although promising, this approach appears rather phenomenological however, and uses questionable assumptions, such as that of solid friction between the particles and the bed.

Keeping to the linear stability analysis followed by Blondeaux (1990), much progress can be made by improving the way the dynamics of the particles is considered. Up to now, this dynamics has been modelled with a semi-empirical algebraic law for the particle flux as a function of the bottom shear stress, as in studies of ripple formation under steady flows (Richards 1980; Sumer & Bakioglu 1984). The aim of this paper is to reconsider the problem using a deeper insight in the particle dynamics, using an erosion–deposition model for a monolayer of particles rolling and sliding over the fixed bed. This model, first introduced in Charru, Mouilleron-Arnould & Eiff (2004) from experiments in an annular Couette device, was used in Part 1 of this paper
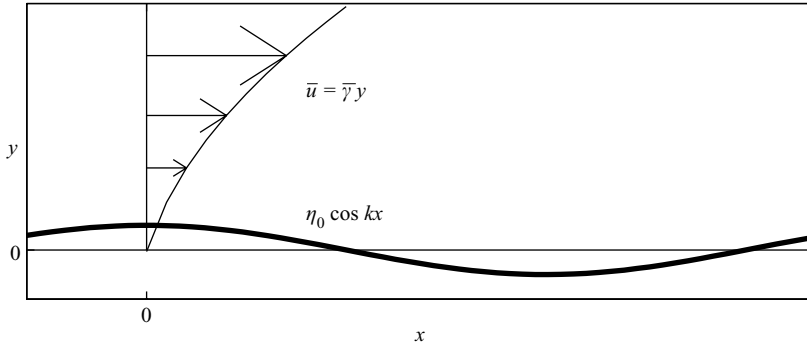
FIGURE 1. Sketch of the fluid layer over a sinusoidal bed, and the base oscillating flow.

(Charru & Hinch 2006) for studying ripple formation in steady flows. It was shown there that, unlike the classical approach, the erosion–deposition model accounts for the observation that increasing the fluid viscosity leads to the disappearance of ripples (Mouilleron 2002). However, these experiments also show that ripples can exist in an oscillating flow when they do not exist in a steady flow. The aim of this paper is to show that the same erosion–deposition also accounts for the latter observation. In addition, we also intend to show that the hydrodynamic instability mechanism is the same for steady flow and oscillating flow.

The paper is organized as follows. The oscillating viscous fluid flow over a sinusoidal bed is calculated analytically in § 2. A simple model of the particle dynamics on a fixed sinusoidal bottom is discussed in § 3, aiming at understanding the difference between steady and oscillating flows. Then the erosion model is presented in § 4. Ripple formation is discussed in § 5, allowing the growth rate to be calculated analytically for long waves. A brief summary is given in § 6.

2. Fluid flow

We consider a fluid layer with density ρ, viscosity μ and thickness h, lying between an erodible bed and a moving upper wall with velocity $U_w \sin \omega t$ (figure 1). The erodible bed is assumed to be perturbed sinusoidally as $\eta = \eta_0 \cos kx$, with wavenumber k and amplitude η_0. Following previous studies, and in agreement with observations, we assume that the time scale of the fluid flow is much shorter than the time scale of the bed evolution. Thus the fluid flow can be calculated as if the wavy bottom were fixed, by considering the flow as the superposition of a base flow $\bar{u}$ over a flat bed, and a disturbance (u, v) induced by the wavy bottom.

When the period of flow oscillation, $2\pi/\omega$, is small compared with the time for momentum to diffuse over the thickness of the fluid layer, $\rho h^2/\mu$, the base flow departs only slightly from a linear shear flow with time-varying shear rate $(U_w/h) \cos \omega t$. The base flow can be found as a power series in the unsteadiness parameter

$$\epsilon_u = \frac{1}{30} \frac{\rho \omega h^2}{\mu}, \tag{2.1}$$

where the numerical factor is introduced for future convenience. At $O(\epsilon_u^2)$, the base flow is found to be, with $Y = y/h$,

$$\bar{u} = U_w(Y \sin \omega t - 5\epsilon_u Y(1-Y)(1+Y) \cos \omega t$$
$$- \tfrac{5}{2}\epsilon_u^2 Y(1-Y)(1+Y)(3Y^2 - 7) \sin \omega t). \tag{2.2}$$

The first term is the quasi-static approximation, and the second and third the dominant inertial corrections. Within this low-frequency approximation, the corresponding shear rate on the bottom is

$$\overline{\gamma} = \Gamma_a \sin(\omega t - \varphi), \qquad \text{with} \quad \Gamma_a = (1 - 10\epsilon_u^2)\frac{U_w}{h}, \quad \varphi = 5\epsilon_u. \tag{2.3}$$

As expected, fluid inertia reduces the amplitude Γ_a, by a factor $(1 - 10\epsilon_u^2)$, and induces a phase lag, φ.

For a wavy bed with wavelength $2\pi/k$ much longer than the fluid thickness, $kh \ll 1$, and small fluid inertia, the longitudinal velocity disturbance can be found as the sum of three contributions:

$$u = \epsilon_0 U_w(u_0 + \epsilon_i u_i + \epsilon_u u_u). \tag{2.4}$$

The first term on the right of (2.4) is the dominant Stokes correction, the second the inertial correction arising from advection effects, and the third the inertial correction due to the base-flow unsteadiness. The small parameters ϵ_0 and ϵ_i measure bottom waviness and advection effects, respectively, and are defined as

$$\epsilon_0 = \frac{4\eta_0}{h}, \quad \epsilon_i = \frac{kh\,Re}{120} \quad \text{with} \quad Re = \frac{\rho U_w h}{\mu}. \tag{2.5}$$

Expanding the transverse velocity and pressure disturbances similarly, and solving the governing equations with the no-slip conditions at the upper and lower boundaries, one obtains the longitudinal velocity disturbances

$$u_0 = -\tfrac{1}{4}(Y-1)(3Y-1)\sin\omega t\cos kx, \tag{2.6}$$

$$u_i = -Y(Y-1)^2(-3Y^2 - Y + 1)\sin^2\omega t\sin kx, \tag{2.7}$$

$$u_u = -\tfrac{1}{8}(Y-1)(15Y^3 - 25Y^2 - 22Y + 10)\cos\omega t\cos kx. \tag{2.8}$$

The generation of the steady streaming can be understood as follows, with the help of figure 2. When the base flow is from left to right ($\sin\omega t > 0$, figure 2a), the leading-order longitudinal velocity, u_0, is in phase with the bottom. Advection by the base flow of the associated vorticity creates the out-of-phase velocity u_i, as shown in the figure (for more details see Part 1). Note that u_u does not contribute to u_i, because it is only a small correction to u_0 (it is not represented in figure 2a); however, it will be seen in the next section that u_u strongly affects particle motion. When the base flow is from right to left ($\sin\omega t < 0$), the in-phase flow u_0 reverses, as shown in figure 2(b). However, the out-of-phase inertially induced flow u_i is not reversed, since it results from both the leading-order correction flow and advection by the base flow, which both change sign. Averaging over one cycle of the oscillation, the net base flow is zero, the net in-phase disturbance flow is zero too, but the net inertially induced out-of-phase flow, or steady streaming, is non-zero, as shown in figure 2(c). An experimental illustration of such a steady streaming induced by an oscillating flow over a wavy boundary is given by Kaneko & Honji (1979).

From now on, the main flow quantity of interest is the bottom shear rate, which is the sum of the base shear rate $\overline{\gamma}$ given by (2.3) and the shear-rate disturbance γ corresponding to the flow disturbance given by (2.4)–(2.8). Shifting the time origin to absorb the bottom phase lag φ, and introducing the amplitude Γ_a, the bottom shear rate finally is

$$\overline{\gamma} + \gamma = \Gamma_a \sin\omega t + \epsilon_0\Gamma_a(\sin\omega t\cos kx - \epsilon_i\sin^2\omega t\sin kx - \epsilon_u\cos\omega t\cos kx) \tag{2.9}$$
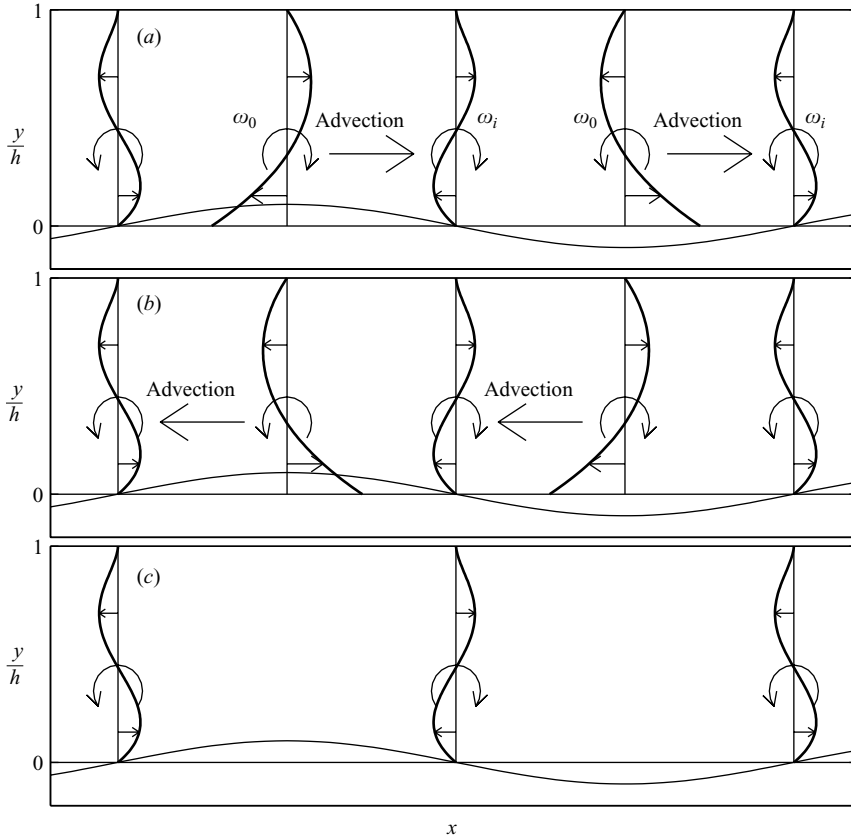
FIGURE 2. (*a*) In-phase and inertially induced out-of-phase flow, when the base flow is from left to right ($\sin \omega t > 0$); (*b*) same as (*a*) but when the base flow is from right to left ($\sin \omega t < 0$); (*c*) net flow averaged over one period (steady streaming).

The four terms on the right-hand side correspond to the base flow, the dominant Stokes correction due to the bottom waviness, and the inertial corrections due to advection and unsteadiness, respectively.

3. A simple model

In this section we study a simple model for the particle motion, which, ignoring any bed erosion or deposition, assumes a constant number of moving particles. The aim of this study is to throw light on an important difference between steady and oscillating flows, and to understand the effects of fluid inertia and oscillation frequency. We consider particles with diameter d, deposited on a wavy fixed bottom (figure 3). We want to know how a uniform initial distribution evolves with time under steady or oscillating flow. Particles are assumed to have no inertia so that their velocity U is proportional to the bottom shear stress $\mu(\overline{\gamma} + \gamma)$. The order of magnitude of U is expected to be the typical fluid velocity $(\overline{\gamma} + \gamma)d$ at a height d above the bottom, where the bottom shear rate $\overline{\gamma} + \gamma$ is given by (2.9). Thus U can written as

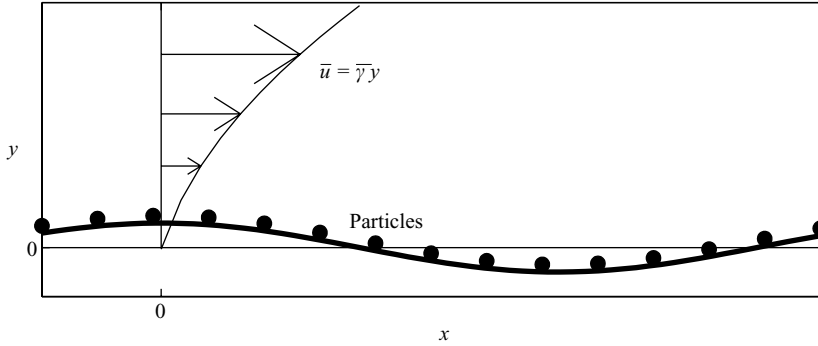$$U = \alpha(\overline{\gamma} + \gamma)d, \tag{3.1}$$

FIGURE 3. Sketch of particles initially deposited on a wavy bottom.

where α is a dimensionless coefficient of order one. This coefficient can be obtained from calculations of the lubrication flow around a smooth particle translating and rotating in a linear shear flow close to a flat wall (Goldman, Cox & Brenner 1967). For particles rolling without slip, with surface roughness $\delta_r = 0.01d$, this coefficient is found to be $\alpha = 0.23$, in agreement with experiments for small shear stress (King & Leighton 1997).

The position $x(t)$ of a particle starting from $x(0) = x_0$ can be obtained from numerical integration of the trajectory equation

$$\frac{\mathrm{d}x}{\mathrm{d}t} = U(x, t), \tag{3.2}$$

where the velocity is given by (3.1). Taking as the length scale the inverse wavenumber k^{-1}, and as the time scale the time needed for a particle with velocity $\alpha \bar{\gamma} d$ to travel distance k^{-1}, we define the dimensionless space and time as

$$X = kx, \quad T = \alpha k d \Gamma_a t. \tag{3.3}$$

Note that usually, for sand ripples under water for example, the amplitude of the particle motion during one cycle is small compared to the wavelength. This corresponds to high dimensionless frequency,

$$\Omega = \frac{\omega}{\alpha \Gamma_a k d} \gg 1. \tag{3.4}$$

With these scales, the particle motion equations (2.9)–(3.2) become

$$\frac{\mathrm{d}X}{\mathrm{d}T} = \sin \Omega T + \epsilon_0 (\sin \Omega T \cos X - \epsilon_i \sin^2 \Omega T \sin X - \epsilon_u \cos \Omega T \cos X). \tag{3.5}$$

The rest of this section is devoted to the numerical investigation of (3.5), which depends on the four parameters Ω, ϵ_0, ϵ_i and ϵ_u.

Figure 4 displays the evolution $x(t)$ of a few particles initially equally spaced on the bottom, for the case of steady flow (which can be obtained from (3.5) by setting $\sin \Omega T = 1$ and $\epsilon_u = 0$). Figure 4(a) corresponds to when inertia is ignored ($\epsilon_i = 0$), whereas figure 4(b) corresponds to non-zero inertia ($\epsilon_i = 1$). In both cases, it can be seen that, as expected, particles tend to gather where the velocity gradient is negative (i.e. down the slopes for small ϵ_i), and they tend to separate where the velocity gradient is positive. However there is no net accumulation near crests or troughs, irrespective of fluid inertia.
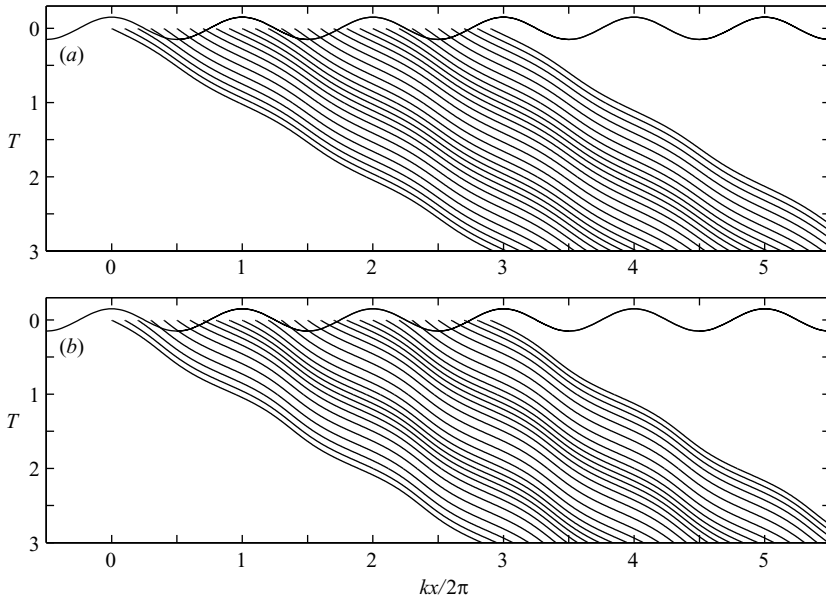
FIGURE 4. Spatio-temporal diagram of the motion of particles initially equally spaced in a steady shear flow over a wavy wall, for $\epsilon_0 = 0.2$. (a) $\epsilon_i = 0$ (no fluid inertia); (b) $\epsilon_i = 1$. The upper sinusoidal trace represents the bed.

Figure 5 displays particle trajectories, as in figure 4, for the case of an oscillating flow with $\Omega = 1$. Figure 5(a) shows that when both the advection and unsteadiness are ignored ($\epsilon_i = 0$, $\epsilon_u = 0$), particles oscillate, but no accumulation is observed, as for the steady flow. Figure 5(b) shows that when advection only is taken into account ($\epsilon_i = 1$, $\epsilon_u = 0$), particles tend to gather upon the crests. Finally, figure 5(c) shows that when unsteadiness only is taken into account ($\epsilon_i = 0$, $\epsilon_u = 1$), particles tend to gather in the troughs. Therefore, it appears that advection and unsteadiness both induce particle drift, but in opposite directions. The net effect depends on the oscillation frequency.

The effect of the oscillation frequency is shown in figure 6, with both inertial effects taken into account ($\epsilon_i = \epsilon_u = 1$). For $\Omega = 1$ (figure 6a), it appears that the net particle drift is zero: the two inertia effects compensate, as might be guessed from figure 5(b, c). However, for the higher frequency $\Omega = 5$ (figure 6b), particles clearly accumulate on the crests. This phenomenon is enhanced at higher frequencies. Thus, in the high-frequency (or long-wave) limit, $\Omega \gg 1$, which, as noted above, corresponds to the usual physical case, the effect on particle motion of the base-flow unsteadiness is negligible, and advection dominates.

The accumulation of the particles on crests in the high-frequency (or long-wave) limit can be better understood from an approximate analytical solution of (3.5). Assuming $1/\Omega \sim \epsilon_0 \sim \epsilon_i \sim \epsilon_u \ll 1$, one obtains, for the position x of a particle

$$kx \sim kx_0 + \frac{\alpha \Gamma_a kd}{\omega}(1 - \cos \omega t) - \tfrac{1}{2}\epsilon_0 \epsilon_i kd\alpha \Gamma_a t \sin kx_0. \tag{3.6}$$

This equation predicts that (i) the mean position of the particle drifts linearly with time towards the nearest crest, in agreement with the numerical solution displayed in figure 6(b), and (ii) the drift velocity, $-\tfrac{1}{2}\epsilon_0 \epsilon_i \alpha \Gamma_a d \sin kx_0$, does not depend on frequency.
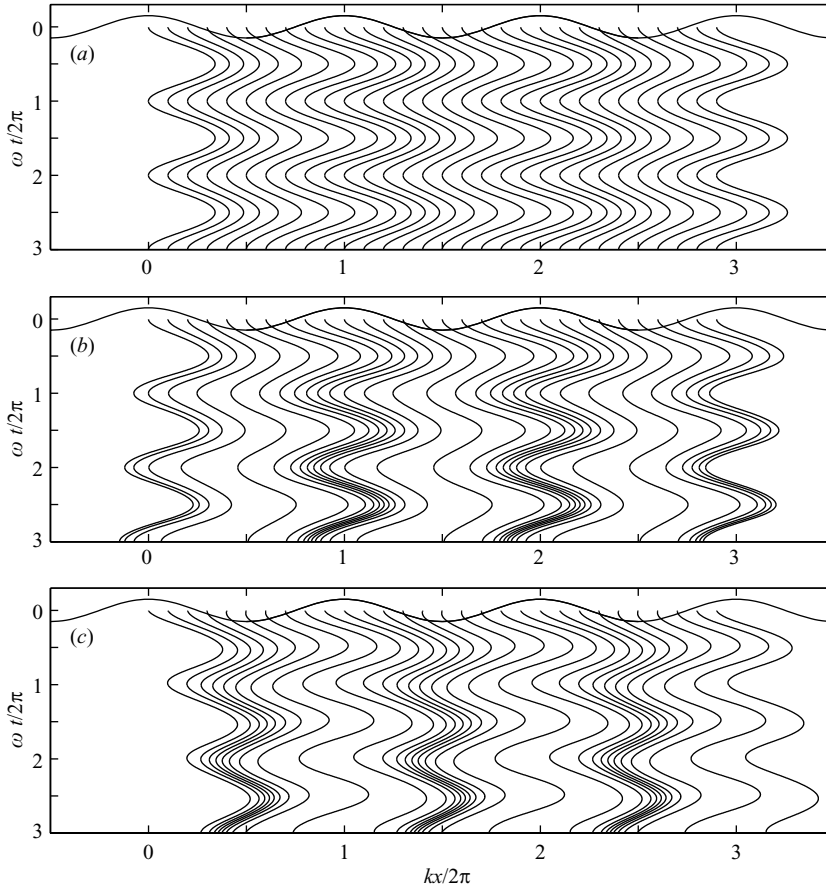
FIGURE 5. Spatio-temporal diagram of the motion of particles initially equally spaced in an oscillating shear flow for $\Omega = 1$ and $\epsilon_0 = 0.2$. (a) $\epsilon_i = 0, \epsilon_u = 0$ (no inertia); (b) $\epsilon_i = 1, \epsilon_u = 0$ (advection only); (c) $\epsilon_i = 0, \epsilon_u = 1$ (unsteadiness only).

From the above equation, the number $n(x, t)$ of particles per unit length can be determined. The particles in the small length dx at time t were in the length dx_0 initially, i.e. $n\,dx = n_0\,dx_0$, where $n_0 = n(x, 0)$ is the initial uniform particle density. Differentiating equation (3.6) and inserting the result into the above Lagrangian conservation equation gives

$$\frac{n}{n_0} \sim 1 + \tfrac{1}{2}\epsilon_0\epsilon_i kd\alpha\Gamma_a t \cos kx. \qquad (3.7)$$

As expected, this equation predicts that, at a fixed location, the number of particles per unit length decreases linearly in the troughs, and increases linearly at the crests. This behaviour is clearly due to the steady-streaming flow shown in figure 2(c).

The conclusion of this analysis reveals an important difference between steady and oscillating flows: in steady flows, the particle density is slightly higher on the lee side of the bed undulation, but it does not vary with time, and the travelling particles successively cross regions of lower and higher density. In oscillating flow, the particle density changes with time, and particles may drift towards troughs or crests, depending on the relative importance of unsteadiness and advection. However, when the amplitude of the particle motion is small compared to the wavelength ($\Omega > 1$), the
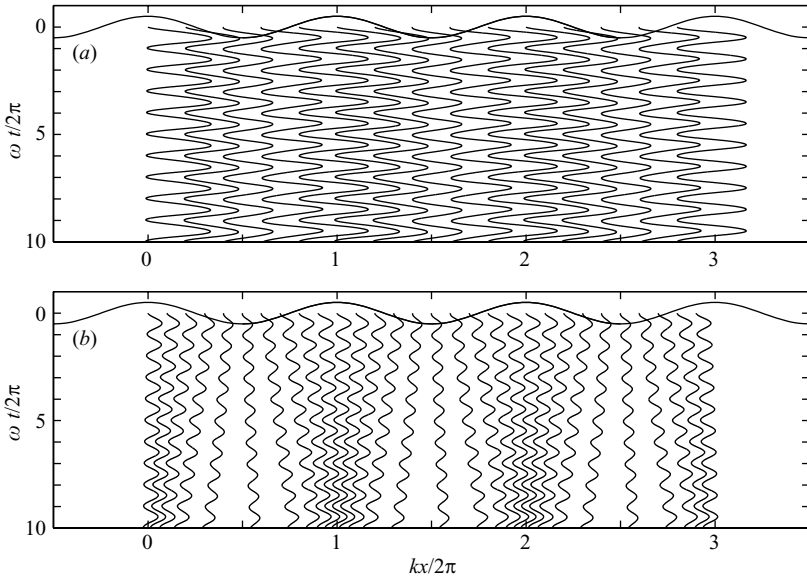
FIGURE 6. Spatio-temporal diagram of the motion of particles initially equally spaced in an oscillating shear flow, for $\epsilon_0 = 0.2$ and $\epsilon_i = \epsilon_u = 1$. (a) $\Omega = 1$; (b) $\Omega = 5$.
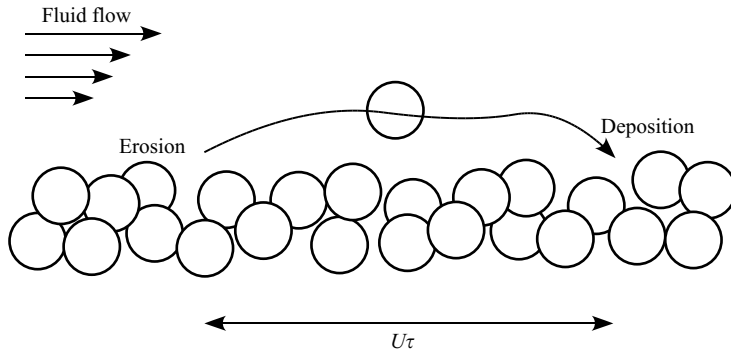

FIGURE 7. Sketch of the erosion and deposition phenomenon.

unsteadiness effect is negligible, the steady-streaming effect dominates, and particles gather on crests. We now turn to the effect of erosion and deposition.

4. An erosion–deposition model

The erosion–deposition model to be presented in this section is essentially the same than that used in Part 1. Thus we just briefly give its main features, emphasizing slight differences. We consider a bed of particles with diameter d and density ρ_p, sheared by a fluid flow with local bottom shear rate $\overline{\gamma} + \gamma$ (figure 7). The condition for particles to be set into motion is that the bottom shear stress $\mu(\overline{\gamma} + \gamma)$ exceeds a threshold $\mu\gamma_{t0}$ (the dependence of this threshold on the local slope will be considered in §5.3). This corresponds to Shields number $\mu(\overline{\gamma} + \gamma)/((\rho_p - \rho)g)d$ higher than a threshold

θ_{t0}, or to normalized Shields number,

$$\Theta = \frac{1}{\theta_{t0}} \frac{\mu(\bar{\gamma} + \gamma)}{(\rho_p - \rho)gd}, \tag{4.1}$$

higher than 1. With the shear rate $(\bar{\gamma} + \gamma)$ defined by (2.9), this normalized Shields number becomes

$$\Theta = \Theta_a \sin \omega t + \epsilon_0 \Theta_a (\sin \omega t \cos kx - \epsilon_i \sin^2 \omega t \sin kx - \epsilon_u \cos \omega t \cos kx), \tag{4.2}$$

where the amplitude Θ_a involves the amplitude Γ_a of the the shear-rate oscillation

$$\Theta_a = \frac{1}{\theta_{t0}} \frac{\mu \Gamma_a}{(\rho_p - \rho)gd}. \tag{4.3}$$

The conservation equation for the number of moving particles per unit bed area, or particle density n, can be written as

$$\frac{\partial n}{\partial t} = -\dot{n}_d + \dot{n}_e - \frac{\partial q}{\partial x}, \tag{4.4}$$

where the variation rate of n is the sum of three terms: the deposition rate $\dot{n}_d$, the erosion rate $\dot{n}_e$, and the divergence of the particle flux q.

The deposition rate $\dot{n}_d$ is modelled as the ratio of the particle density n to a typical duration of saltation flights τ:

$$\dot{n}_d = \frac{n}{\tau} \quad \text{with} \quad \tau = \frac{d}{c_d V_S}, \quad V_S = \frac{(\rho_p - \rho)gd^2}{18\mu}, \tag{4.5}$$

where V_S is the Stokes settling velocity and c_d is a coefficient.

The erosion rate is considered as proportional to $(\bar{\gamma} + \gamma - \gamma_t)/d^2$ where γ_t is the threshold shear rate for particle motion, i.e. proportional to the excess shear rate. Introducing the saltation time τ, the erosion rate can be written as

$$\dot{n}_e = \frac{c_e}{\tau d^2}(|\Theta| - 1)_+, \tag{4.6}$$

where c_e is a coefficient and the subscript $+$ means that $(|\Theta| - 1)$ has to be set to zero when negative (i.e. no erosion below the threshold).

The particle flux q is the product of the particle density n and the mean particle velocity U, which is assumed to be proportional to the fluid velocity $(\bar{\gamma} + \gamma)d$ at a distance d above the bed surface. Then the particle flux can be written as

$$q = \frac{c_u}{\tau d} \Theta(nd^2). \tag{4.7}$$

where c_u is a coefficient.

Choosing the particle diameter d and the jump time τ as the unit length and time, respectively, we define the dimensionless space X and time T, the dimensionless wavenumber K and frequency Ω, and the dimensionless particle density N and particle flux Q, as

$$X = \frac{x}{d}, \quad T = \frac{t}{\tau}, \quad K = kd, \quad \Omega = \omega\tau, \quad N = nd^2, \quad Q = q\tau d. \tag{4.8}$$

Note that this non-dimensionalization differs from that used in §3. The conservation equation (4.4) now becomes

$$\frac{\partial N}{\partial T} = -N + c_e(|\Theta| - 1)_+ \frac{\partial Q}{\partial X}, \quad \text{with} \quad Q = c_u \Theta N, \tag{4.9}$$
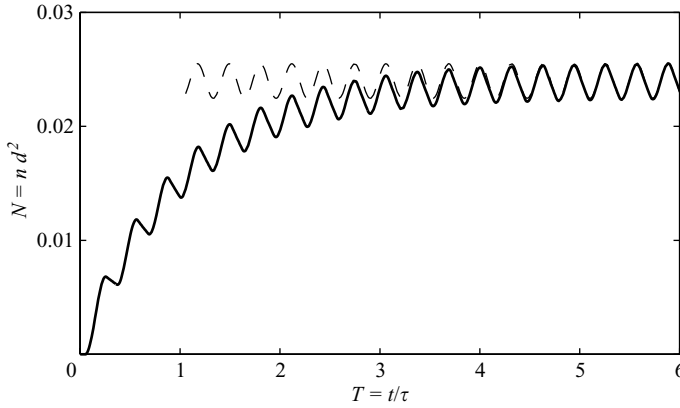
where Θ is given by (4.2).

FIGURE 8. Time evolution of the density of moving particles on a flat bed, starting from rest, for $c_e = 0.055$, $\Omega = 10$ and $\Theta_a = 2$. Solid line: numerical solution of (4.9); dashed line: approximate solution with mean value (5.1) and oscillatory correction given by (5.9).

The erosion and deposition models (4.6) and (4.5), as well as the flux law (4.7) were derived from experiments reported in Charru *et al.* (2004). These steady flow experiments allowed the determination of the coefficients c_e, c_d and c_u, which are assumed to remain the same for oscillating flow:

$$\theta_t = 0.12, \qquad c_e = 0.055, \qquad c_d = 0.067, \qquad c_u = 3.3. \qquad (4.10)$$

In the oscillating experiments of Mouilleron (2002), the frequency of the oscillations was in the range 0.1–1 Hz, and the wavelength of the observed ripples in the range 5–10 cm. This corresponds to a dimensionless wavenumber $K = 0.03$–0.07 and dimensionless frequency $\Omega = 2.5$–25. Therefore the following analysis only considers the case of long waves, $K \ll 1$, and high frequency, $\Omega \gg 1$.

5. Ripple formation

5.1. *Density of mobile particles at high frequency*

First consider the case of a flat bed. The density N of mobile particles results from a local balance between erosion and deposition, and is approximately constant at high frequency. This is illustrated in figure 8, which displays the time evolution of N, starting from rest, obtained by numerical integration of (4.9) with $\epsilon_0 = 0$. After a short transient, N oscillates with frequency 2Ω about its mean value. This mean value can be obtained by time averaging (4.9), giving

$$N \sim c_e A, \qquad (5.1)$$

where A is the mean value of the driving shear stress:

$$A = \overline{(|\Theta| - 1)_+}^t = \frac{2}{\pi} \left(\sqrt{\Theta_a^2 - 1} - \cos^{-1} \frac{1}{\Theta_a} \right). \qquad (5.2)$$

Figure 8 also shows an approximate solution including the leading-order oscillatory correction, of order $1/\Omega$, which will be given later, see equation (5.9). On a wavy bed, a correction of order ϵ_0 should be added, see equation (5.10), corresponding to the fact that the shear stress, and thus N, is slightly higher on the crests than in the troughs.

5.2. *Effect of the steady streaming*

The particle flux associated with the density of mobile particles calculated above in (5.1) is $Q = c_u N \Theta$, with Θ given by (4.2). Averaging over time, the mean flux is found to be

$$\overline{Q}^t \sim c_u \overline{N\Theta}^t \sim -\epsilon_0 \epsilon_i \frac{c_u c_e}{2} A \Theta_a \sin KX. \tag{5.3}$$

Note that the $O(1/\Omega)$ oscillatory correction to N, as well as the corrections due to the wavy bed, lead to higher-order corrections to the above mean flux. This flux, directed up to the crests, arises from the contribution of advection to the shear stress, which is the only one with non-zero mean, i.e. it is driven by the steady-streaming flow shown in figure 2. This flux is responsible for the growth of the disturbance.

5.3. *Effect of gravity*

On a wavy bed, gravity pulls the particles towards troughs, with a force parallel to the bed equal to $(\rho_p - \rho)g\partial_x \eta$ per unit volume. This force has two effects, both stabilising: it modifies the threshold Shields number for particle motion, and it induces a falling velocity of mobile particles from crests to troughs. These two effects give separate contributions to the growth rate. However, since these contributions are qualitatively the same, as shown in Part 1, and considering the uncertainty involved the numerical coefficients, here we only take into account the falling-velocity effect for the sake of simplicity. This falling velocity along the bed surface is expected to be proportional to $-V_S \partial_x \eta$, and can be written as $U_g = (d/\tau)c_g \epsilon_0 kh \sin kx$, where c_g is a coefficient. The corresponding particle flux is $q_g = U_g n$, or, in dimensionless form, $Q_g = (U_g \tau/d)N$, where the particle density N is given by (5.1). The time-averaged dimensionless flux due to gravity finally is

$$\overline{Q_g}^t = \epsilon_0 kh c_g c_e A \sin KX. \tag{5.4}$$

As expected this flux drives the particles from the crests down to the troughs.

5.4. *Erosion of the peaks*

The above analysis includes two major phenomena: the steady streaming due to fluid inertia, which is destabilising, and the gravity flux, which is stabilising. However, another effect may be important, to which this section is devoted. The study of steady flow in Part 1 revealed that higher erosion on the crests due to higher shear stress, and transport by the base flow of the particles eroded there, lead to particle deposition in troughs; this stabilising phenomenon can overcome the destabilising effect of fluid inertia, so that the flat bed may be stable for any Shields number. This phenomenon also exists in oscillating flow: while oscillating on a wavy bed, the particles explore regions of higher and lower shear stress, at the upper and lower part of their trajectory, respectively. Thus, some of the particles which were mobile at their upper position, closer to the crest, are deposited as they reach their lower position, closer to the trough. The above effect results in a net migration of the particles from crests to troughs. The aim of this section is to analyse more precisely this phenomenon, which, although it is physically obvious, its calculation is less obvious. For the sake of simplicity, we ignore inertia effects, which are not essential here, and set $\epsilon_i = \epsilon_u = 0$.

The method consists of solving (4.9) by a long-wave expansion of the density N and the flux Q,

$$N = \overline{N} + \epsilon_0 \big(N^{(0)} + K N^{(1)} + K^2 N^{(2)} + \cdots\big), \tag{5.5}$$

$$Q = \overline{Q} + \epsilon_0 \big(Q^{(0)} + K Q^{(1)} + K^2 Q^{(2)} + \cdots\big). \tag{5.6}$$

The forcing term $(|\Theta| - 1)_+$ in (4.9) will be approximated by a Fourier expansion retaining the mean term and the dominant harmonic with frequency 2Ω:

$$(|\Theta| - 1)_+ \sim A + \epsilon_0 A' \cos KX + \frac{B + \epsilon_0 B' \cos KX}{2\Omega} \cos 2\Omega T, \qquad (5.7)$$

where
$$A = \frac{2}{\pi} \left(\sqrt{\Theta_a^2 - 1} - \cos^{-1} \frac{1}{\Theta_a} \right),$$

$$A' = \Theta_a \frac{\mathrm{d}A}{\mathrm{d}\Theta_a} = \frac{2}{\pi} \sqrt{\Theta_a^2 - 1},$$

$$B = -\frac{4\Theta_a}{3\pi} \left(1 - \frac{1}{\Theta_a^2} \right)^{3/2},$$

$$B' = \Theta_a \frac{\mathrm{d}B}{\mathrm{d}\Theta_a} = -\frac{4}{3\pi} \sqrt{\Theta_a^2 - 1} \frac{\Theta_a^2 + 2}{\Theta_a^2}.$$

The base-flow particle density $\overline{N}$ is governed by

$$\frac{\partial \overline{N}}{\partial T} = -\overline{N} + c_e \left(A + \frac{B}{2\Omega} \cos 2\Omega T \right), \qquad (5.8)$$

with the following solution for high frequency:

$$\overline{N} \sim c_e \left(A + \frac{B}{2\Omega} \sin 2\Omega T + \frac{B}{(2\Omega)^2} \cos 2\Omega T \right). \qquad (5.9)$$

This is the expression plotted in figure 8, where it appears that it is a good approximation of the exact numerical solution. This would not be the case for shear-stress amplitude very close to threshold, i.e. $\Theta_a - 1 \ll 1$, where the duration of the particle motion is a small fraction of the oscillation period, so that higher harmonics cannot be neglected.

At $O(\epsilon_0 K^0)$, the equation to be solved is similar to (5.8), with $A' \cos KX$ and $B' \cos KX$ instead of A and B, with solution

$$N^{(0)} \sim c_e \left(A' + \frac{B'}{2\Omega} \sin 2\Omega T + \frac{B'}{(2\Omega)^2} \cos 2\Omega T \right) \cos KX. \qquad (5.10)$$

Note that the oscillating part has to be retained in the present analysis up to the second order. Indeed, for infinite frequency, the amplitude of the oscillations of the particles is zero, and the peaks cannot be eroded by the mechanism sketched at the beginning of this section. Moreover, the following analysis shows that the $O(1/\Omega)$-correction is not sufficient, and that the $O(1/\Omega^2)$-terms have to be retained. The particle flux associated with $N^{(0)}$ is $Q^{(0)} = c_u N^{(0)} \Theta$, with zero mean value $\overline{Q^{(0)}}^t$, so that the higher order has to be calculated. Incidentally, note that if the inertial terms were retained in the present K-expansion, the mean flux (5.3) calculated before would be recovered at this $O(\epsilon_0 K^0)$, with a finite-frequency correction of order $\epsilon_0 \epsilon_i / \Omega^2$.

At the following $O(\epsilon_0 K^1)$, the correction $N^{(1)}$ of the density of mobile particles is found as the sum of three terms, involving $\sin \Omega T$, $\cos \Omega T$ and $\sin 3\Omega T$, with the same spatial dependence in $\sin KX$. A non-zero mean flux $\overline{Q^{(1)}}^t$ arises from the $\sin \Omega T$ term, equal to

$$\overline{Q^{(1)}}^t = c_u \overline{N^{(1)} \Theta}^t$$
$$= \frac{c_e c_u^2 \Theta_a^2}{2\Omega^2} \left(A + A' + \tfrac{1}{4}(B + B') \right) \sin KX. \qquad (5.11)$$

As expected from the physical analysis at the beginning of this section, the above crest-erosion flux drives the particles from the crests down to the troughs, and is stabilising. However, it appears that its order of magnitude is ϵ_0/Ω^2, which has to be compared with that of the steady-streaming flux (5.3), which is $\epsilon_0\epsilon_i$. Thus, for high frequency, such that $\Omega > 1/\epsilon_i$, crest erosion is smaller than steady streaming by one order of magnitude, so that it is negligible. It is also negligible compared to the gravity effect, by a factor $1/(\Omega^2 kh)$.

5.5. *Growth rate*

The mean net erosion–deposition rate can be obtained by averaging (4.9) over time, giving

$$\tau d^2 \overline{(\dot{n}_d - \dot{n}_e)}^t = -\frac{\partial \overline{Q}^t}{\partial X} - \frac{\partial \overline{Q_g}^t}{\partial X}, \tag{5.12}$$

where $\overline{Q}$ is the steady-streaming flux given by (5.3), and $\overline{Q_g}$ is the gravity contribution (5.4). The crest-erosion contribution (5.11) has been omitted since it is negligible at high frequencies. This net erosion–deposition rate is related to the time variation of the bed surface by

$$\frac{\partial \eta}{\partial t} = \frac{\pi d^3}{6\phi} \overline{(\dot{n}_d - \dot{n}_e)}^t, \tag{5.13}$$

where ϕ is the volume fraction of the particles on the bed. Then the growth rate is found to be

$$\sigma = \frac{1}{\tau} \frac{2\pi}{3\phi} c_e A(kd)^2 \left(c_u \frac{Ga\theta_{t0}}{240} \frac{h^2}{d^2} \Theta_a^2 - c_g \right). \tag{5.14}$$

In the above equation, A is the mean value of the effective Shields number $(|\Theta|-1)_+$, given by (5.2), and the Galileo number is defined as

$$Ga = \frac{\rho_p - \rho}{\rho} \frac{\rho^2 g d^3}{\mu^2}, \tag{5.15}$$

which does not depend on the shear rate. Note that there is no wave drift here, since the steady streaming has no uniform component, as it is the case for oscillating flow created by a travelling surface wave (Faraci & Foti 2001).

Thus, there exists a threshold Shields-number amplitude Θ_{ac} above which the stabilizing effect of gravity is overcome by the steady-streaming effect, so that long waves are unstable, with growth rate scaling as the square of the wavenumber. For high Galileo number (typically large particle diameter or small viscosity), Θ_{ac} is lower than 1, so that the bed is unstable as soon as particles move. For small Galileo number, Θ_{ac} is higher than 1, so that there exists a Shields-number range in which particles move over a stable flat bed.

6. Summary and discussion

As explained in the introduction, the ripple formation models used up to now for oscillatory flows, such that of Blondeaux (1990), are based on a decoupling of the time scales for the fluid flow and the bed evolution: the fluid flow is calculated as if the wavy bed were fixed, and the bed evolution is then calculated from an algebraic power law for the particle flux as a function of the bottom shear rate. The main weakness of this approach is the approximate way in which the particle dynamics is treated. In particular, this approach cannot account for the observation that a

higher shear stress on the crests implies more erosion and the flattening of the bed. In the present study, we have proposed a more elaborate description of the particle dynamics, based on an erosion–deposition model. In particular, this model accounts for the crest-erosion phenomenon.

The erosion–deposition model, together with asymptotic expressions for the fluid flow, allows an analytic derivation of the net deposition rate and growth rate, when the oscillation period is short compared to the duration of particle flights over the bed, i.e. for high dimensionless frequency Ω. This limit also corresponds to small amplitude of the particle motion compared to the wavelength. Within this limit, it appears that the dominant contributions to the growth rate are the destabilizing effect of the steady streaming and the stabilising effect of gravity. The contribution of crest erosion is smaller by one order of magnitude when $1/\Omega$ and the small parameter ϵ_i, which is an effective Reynolds number, are of the same order of magnitude. The net effect of the steady streaming and gravity is that the bed is unstable above a critical Shields number Θ_a given by (5.14) with $\sigma = 0$. For high Galileo number, Θ_a is lower than the threshold for particle motion, so that the bed is unstable as soon as particles are set into motion. For small Galileo number, a range of stable Shields number exists beyond the threshold.

The above results imply that for a bed of particles sheared by an oscillating viscous flow, there always exists a critical Shields number above which the flat bed is unstable. This result contrasts with that for steady flow in Part 1, according to which for small Galileo number (typically small particle diameter or high viscosity), the crest-erosion phenomenon dominates advection, so that the bed is stable whatever the Shields number. These predictions for steady and oscillating flow both agree with experiments by Mouilleron (2002). In these experiments, in an annular Couette-flow device described in Charru *et al.* (2004), ripples were not observed in a steady flow for a viscosity higher than 26×10^{-3} Pa s, corresponding to $Ga < 1.1$, whereas they were still observed to grow in oscillating flow, at least for a viscosity up to 100×10^{-3} Pa s which was the highest tested viscosity.

Finally, the present analysis, which is valid for waves longer than the fluid depth, cannot predict any wavenumber selection. Indeed the predicted growth rate (5.14) scales as the square of the wavenumber, as for the steady flow case. However, this analysis could be easily extended to short waves, within the framework of the same erosion–deposition equation (4.9), by using the short-wave flow parameters ϵ_0 and ϵ_i given in Part 1. Again, one might expect the maximum growth rate to occur around $kh = O(1)$.

REFERENCES

ANDERSEN, K. H. 2001 A particle model of rolling grain ripples under waves. *Phys. Fluids* **13**, 58–64.

BAGNOLD, R. 1946 Motion of waves in shallow water. Interaction between waves and sand bottoms. *Proc. R. Soc. Lond.* A **187**, 1–18.

BLONDEAUX, P. 1990 Sand ripples under sea waves. Part 1. Ripple formation. *J. Fluid Mech.* **218**, 1–17.

CHARRU, F. & HINCH, E. J. 2006 Ripple formation on a particle bed sheared by a viscous liquid. Part 1. Steady flow. *J. Fluid Mech.* **550**, 111–121.

CHARRU, F., MOUILLERON-ARNOULD, H. & EIFF, O. 2004 Erosion and deposition of particles on a bed sheared by a viscous flow. *J. Fluid Mech.* **519**, 55–80.

FARACI, C. & FOTI, E. 2001 Evolution of small scale regular patterns generated by waves propagating over a sandy bottom. *Phys. Fluids* **13**, 1624–1634.

GOLDMAN, A. J., COX, R. G. & BRENNER, H. 1967 Slow viscous motion of a sphere parallel to a plane wall - II Couette flow. *Chem. Engng Sci.* **22**, 653–660.

KANEKO, A. & HONJI, H. 1979 Double structures of steady streaming in the oscillatory viscous flow over a wavy wall. *J. Fluid Mech.* **93**, 727–736.

KING, M. R. & LEIGHTON, D. T. 1997 Measurement of the inertial lift on a moving sphere in contact with a plane wall in a shear flow. *Phys. Fluids* **9**, 1248–1255.

MOUILLERON, H. 2002 Instabilités d'un milieu granulaire cisaillé par un fluide. Thèse de Doctorat, Université Paul Sabatier, Toulouse, France.

RICHARDS, K. J. 1980 The formation of ripples and dunes on an erodible bed. *J. Fluid Mech.* **99**, 597–618.

SLEATH, J. F. A. 1976 On rolling-grain ripples. *J. Hydraul. Res.* **14**, 69–81.

STEGNER, A. & WESFREID, J. E. 1999 Dynamical evolution of sand ripples under water. *Phys. Rev. E* **60**, 3487–3490.

SUMER, B. M. & BAKIOGLU, M. 1984 On the formation of ripples on an erodible bed. *J. Fluid Mech.* **144**, 177–190.